nature nanotechnology

ARTICLES

PUBLISHED ONLINE: 22 JUNE 2014 | DOI: 10.1038/NNANO.2014.117

Metamaterial mirrors in optoelectronic devices

Majid Esfandyarpour[1], Erik C. Garnett[1†], Yi Cui[1,2], Michael D. McGehee[1] and Mark L. Brongersma[1]*

The phase reversal that occurs when light is reflected from a metallic mirror produces a standing wave with reduced intensity near the reflective surface. This effect is highly undesirable in optoelectronic devices that use metal films as both electrical contacts and optical mirrors, because it dictates a minimum spacing between the metal and the underlying active semiconductor layers, therefore posing a fundamental limit to the overall thickness of the device. Here, we show that this challenge can be circumvented by using a metamaterial mirror whose reflection phase is tunable from that of a perfect electric mirror ($\varphi = \pi$) to that of a perfect magnetic mirror ($\varphi = 0$). This tunability in reflection phase can also be exploited to optimize the standing wave profile in planar devices to maximize light–matter interaction. Specifically, we show that light absorption and photocurrent generation in a sub-100 nm active semiconductor layer of a model solar cell can be enhanced by ~20% over a broad spectral band.

Mirrors have a long and colourful history in the field of optics, and their earliest use dates back at least 8,000 years[1]. Currently they are key components in complex optical systems and are used as back reflectors in a wide range of devices. One major drawback of metallic mirrors in planar optoelectronic devices becomes obvious when an active semiconductor layer is placed in direct contact with the metal. When light reflects off a high-conductivity metal mirror, the electric field strength in the region within about one-quarter wavelength ($\lambda/4$) of the metal is significantly lowered. This is a direct consequence of the boundary conditions for the electric and magnetic fields at a planar semiconductor/metal interface, which prescribe that, in response to an incident light wave, a back-reflected wave will be generated with an electric field that opposes the electric field of the incident wave (Fig. 1a). As the magnitude of the local electric field determines the strength of the light–matter interaction, it is clear that this interaction is suppressed near the mirror surface. This is therefore a particularly significant problem in devices with deep subwavelength active layers, especially as such thin devices are becoming increasing prevalent as they offer substantive benefits in terms of decreased materials usage, costs and processing times, as well as increased performance in terms of speed of operation and charge injection/extraction properties. To circumvent this issue it would be desirable to use a different type of mirror that has its highest electric field right at its surface. Such a mirror is termed a 'magnetic mirror'[2]. Magnetic mirrors naturally accomplish this feat by flipping the magnetic field of an incident light wave, rather than the electric field, upon reflection (Fig. 1a–c).

When optimizing the light–matter interaction in devices it is important not only to control the spatial distribution of the electric field in the active layers, but also to maximize the overall intensity. In devices with planar semiconductor layers the field intensity can be increased by capitalizing on optical resonances to facilitate the effective recirculation of light (Supplementary Fig. 1). Metal films serving as back reflectors can be used to manipulate both the field distribution and the optical resonances by controlling the reflection phase of the incident light waves. Recent work has capitalized on this notion to achieve strongly enhanced light absorption in semiconductor films less than one-quarter wavelength in thickness[3,4].

Design of metamaterial mirrors

In this Article we show how highly reflective metamaterial mirrors with any desired reflection phase can be realized and implemented in devices operating in the visible spectral range. To understand how the properties of a conventional metallic mirror can be manipulated to produce a specific reflection phase of interest, we analyse the complex reflection coefficient for a light wave bouncing off a reflecting surface:

$$r = r_0 e^{i\varphi} = \frac{Z_S - \eta_m}{Z_S + \eta_m} \quad (1)$$

where r_0 and φ are the reflection amplitude and phase, η_m is the characteristic impedance of the incident medium, and Z_S is the surface impedance of the reflector surface. The characteristic impedance of the medium is determined by its permeability μ_m and permittivity ε_m as $\eta_m = \sqrt{\mu_m/\varepsilon_m}$. The magnitude of Z_S follows from Ohm's law and is given by the ratio of the tangential electric and magnetic fields at the reflector surface. Its magnitude is expressed in ohm per square. A high-conductivity metal forces the electric field to zero at its surface and thus features a low Z_S. For this reason, a reflected wave experiences a complete phase reversal ($\varphi \approx \pi$). However, by judiciously patterning the metal surface with subwavelength-scale structures one can engineer the surface impedance and thus the reflection phase.

The design of our metamaterial mirror was inspired by the work of Sievenpiper[5] on high-impedance surfaces and the many activities in the microwave and optical regimes to control the reflection phase of mirrors by using engineered metamaterial surfaces known as metasurfaces. Metasurfaces are built up from two-dimensional subwavelength metallic building blocks and demonstrate unique responses to the incoming light that transcend those of natural materials[6–22]. A wide variety of metallic structures have been implemented in the design of metasurfaces, including space filling curves like Hilbert curves[13], mushroom-like electromagnetic bandgap surfaces[14], planar chiral structures[15,16], fish-scale structures[17,18] and nanoantenna arrays[19–21]. Of particular relevance to this work are recent studies on metasurfaces that serve as magnetic mirrors[4], efficient broadband wave retarders[16] or enable spectral control over reflected light intensity at optical frequencies[10,22].

[1]Geballe Laboratory for Advanced Materials, Stanford University, 476 Lomita Mall, Stanford, California 94305, USA, [2]Stanford Institute for Materials and Energy Sciences, SLAC National Accelerator Laboratory, 2575 Sand Hill Road, Menlo Park, California 94025, USA, †Present address: Center for Nanophotonics, FOM institute AMOLF, Science Park 104, 1098 XG, Amsterdam, the Netherlands. *e-mail: brongersma@stanford.edu

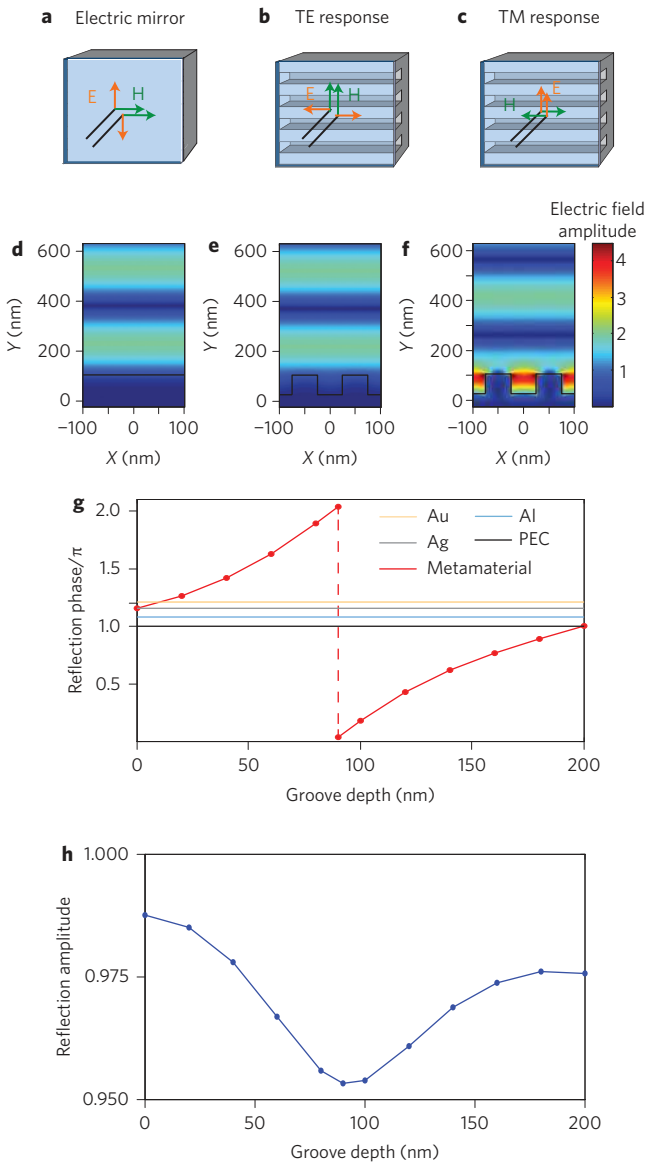

Figure 1 | Optical properties of a metamaterial mirror. a–c, Difference in the optical behaviour of a conventional mirror (**a**) and a metamaterial mirror that for one polarization behaves as an electric mirror that flips the electric field of an incident light wave on reflection (**b**) and for the other polarization serves as a magnetic mirror capable of flipping the magnetic field (**c**). This type of mirror can be realized by patterning a subwavelength groove array into a smooth metal film. **d–f**, Simulated electric field amplitude distributions are shown for 600-nm-wavelength light reflecting from a conventional flat silver mirror (**d**) and a grooved silver mirror under transverse electric (TE; **e**) and transverse magnetic (TM; **f**) illumination. TM illumination gives rise to magnetic mirror behaviour and produces a maximum in the electric field intensity at the top of the grooves. The field is normalized by the field amplitude of the incident plane wave. **g**,**h**, Plots of the dependence on groove depth of the reflection phase (**g**) and amplitude (**h**) for light at 600 nm reflecting from a patterned mirror. The reflection phases for a perfect electrical conductor (PEC), Al, Ag and Au are shown for comparison (**g**).

Based on the above works we decided to pattern a nanoscale groove array into a conventional metallic mirror to produce a metamaterial mirror whose properties can be described by an effective surface impedance that is different from that of a smooth metal surface. The grooves force the surface currents in the metal to follow more tortuous paths and thus change the effective surface impedance and reflection phase. This can significantly increase the surface impedance compared to a smooth metal, and the magnitude of Z_S can be accurately controlled through the choice of groove dimensions. For example, equation (1) shows that a mirror with very high Z_S will produce a reflected wave with negligible phase pick-up ($\varphi \approx 0$), mimicking the properties of a magnetic mirror.

The design of the grooved metamaterial mirror is somewhat modified from its radiofrequency counterpart, as subwavelength grooves in the optical regime support surface plasmon resonances[23,24]. For example, this can be observed in the possibility of realizing black metals with a dense array of convex grooves[25]. We illustrate the effect grooves can have on the reflection of light with full-field simulations. Figure 1d shows how the reflection of normally incident, 600 nm light from a conventional, planar silver mirror results in a standing wave with a suppressed electric field near its surface. A very similar field profile results when a mirror with a periodic groove array featuring 50-nm-wide and 80-nm-deep grooves is illuminated with transverse electric (TE)-polarized light (Fig. 1e). The situation changes dramatically when the grooved mirror is illuminated with transverse magnetic (TM)-polarized light (Fig. 1f). For this polarization the field profile shifts by a quarter wavelength and a standing wave with a maximum electric field right at the surface of the teeth is produced, precisely as expected for a magnetic mirror.

The critical importance of the groove dimensions in the overall design of the magnetic mirror can be understood in more depth by realizing that its operation relies on magnetoelectric interference of the illuminating plane wave and the scattered field by patterned grooves[24]. This facilitates efficient coupling of the incident plane wave to the gap surface plasmon polariton (SPP) modes supported by the grooves and an effective funnelling of light into the grooves. The gap SPPs subsequently reflect off the bottom of the grooves and ultimately couple back to free-space propagating modes. This last step produces the back-reflected wave (Supplementary Fig. 2a–d).

Figure 1g,h shows how the depth of the grooves can be chosen to realize any desired reflection phase with relatively low optical losses in the mirror. The reflection phases for several commonly used metals at the considered wavelength of 600 nm are also shown. It can be seen that the reflection phases of high-conductivity metals are limited to a narrow range of values slightly greater than π. As the reflection phase is controlled by the gap SPPs that pick up phase while propagating up and down the grooves, the observed close-to-linear change in the phase pick-up with groove depths is expected. This aspect allows one to modify the reflector properties from a perfect electric mirror (π reflection phase) to a perfect magnetic mirror (0 reflection phase) by simply changing the groove depth from 80 to 190 nm. The reflection phase for a real metal is not exactly equal to π, as can be seen from the non-zero field near a flat mirror (Fig. 1d). Based on the optical properties of a given metal, the reflection phases that are obtained at different wavelengths are fixed. By subwavelength nanopatterning, the phase pick-up becomes a quantity that can be engineered to any desired value at any target operation wavelength. This type of ability to realize metals with new optical properties that are not found in nature is at the core of the metamaterials field.

Implementing a metamaterial mirror in a device

In the next step we implement a metamaterial mirror into a model organic solar cell featuring an 80-nm-thin (subwavelength) organic semiconductor layer. To maximize the absorption in such a thin semiconductor layer one needs to realize a favourable electric field distribution with good spatial overlap with the absorbing medium and drive an optical resonance to increase the overall field intensity. For devices with very thin layers, the reflection phases can exceed

the roundtrip propagation phase on resonance and become a very important design parameter. This insight has recently led to the demonstration of omnidirectional resonances in planar metallic cavities[26,27] and extremely strong absorption in ultrathin, deep-sub-wavelength semiconductor layers[2,28] as well as patterned metal[29] and graphene films[30] above a metallic mirror. With the introduction of patterned mirrors offering arbitrary reflection phases, optical resonances can now be engineered for any device thickness and any operation wavelength, without the need for optical spacers (Supplementary Fig. 1). This includes cavity dimensions that are deep subwavelength, that is, much less than the typical minimum thickness of $\lambda/2$ for cavities with high-conductivity metallic mirrors.

The inset to Fig. 2a shows one of the periodically repeated unit cells of the proposed device structure. It features a bulk heterojunction poly[*N*-9′-heptadecanyl-2,7-carbazole-alt-5,5-(4′,7′-di-2-thienyl-2′,1′,3′-benzothiadiazole)]:[6,6]-phenyl C_{70}-butyric acid methyl-ester (PCDTBT:$PC_{70}BM$) absorber layer with a thickness of 80 nm. This layer thickness was found to be close to optimal for a device with a conventional silver mirror[31]. Cells with thicker absorption layers can absorb more light, but their overall performance is not improved as the low mobility of the charges in the active layer prevents effective carrier collection. The PCDTBT:$PC_{70}BM$ layer is surrounded by a 5-nm-thick ZnO layer and a 40-nm-thick poly(3,4-ethylenedioxythiophene) (PEDOT) layer that facilitate effective charge extraction. To improve light absorption in the bulk heterojunction, we designed a metamaterial mirror consisting of a periodic array of 105-nm-wide and 160-nm-deep grooves carved into the silver back reflector. The simulated absorption spectra for devices with both types of reflector are shown in Fig. 2a. To calculate the light absorption in the device with the metamaterial mirror, the field magnitudes in the active layer were averaged over one of the periodically repeating unit cells. A broadband absorption enhancement can be observed for the metamaterial-mirror device in the target range from ~500 nm to 700 nm, where the contributions to the short-circuit current of the cell are greatest. We found that the light absorption at a specific wavelength could be further enhanced by changing the groove dimensions, but only at the cost of reducing the overall broadband absorption in the targeted wavelength range. The origin of this broadband enhancement is analysed in the next paragraph.

Figure 2b–f shows the evolution of the electric field distributions in the active layer (red), the PEDOT layer (blue) and above two devices as the illumination wavelength is increased from 500 nm to 700 nm. From an analysis of this evolution, it can be understood how the device with the metamaterial mirror can deliver a broadband enhancement in the light absorption across this wavelength range. At 500 nm, the metamaterial mirror produces the same reflection phase (modulo 2π) as the smooth silver mirror. This is because the groove depth of 160 nm is approximately equal to half a gap SPP wavelength. As a result, the incident light accumulates 2π phase in making one roundtrip in the groove. By having the same reflection phase for the two mirrors, the field profile above these mirrors and the absorption in the active layer are also the same. The field profile at 500 nm shows that the field maximum is desirably located in the centre of the active layer, and this results in a strong absorption of 80% of the incident photons. At longer wavelengths (up to 700 nm), the average field intensity in the active layer is larger for the device with the metamaterial mirror. This is due to the fact that the metamaterial mirror allows the device to operate closer to resonance by providing the desired reflection phase. This allows for an improved resonant recirculation of the light that increases the overall field intensity and thus the light absorption. The enhanced absorption in the device with the metamaterial mirror can also be seen in the reduced amplitude of the standing wave above the device, which would go to zero if all the light were absorbed in the device. It is worth noting that the

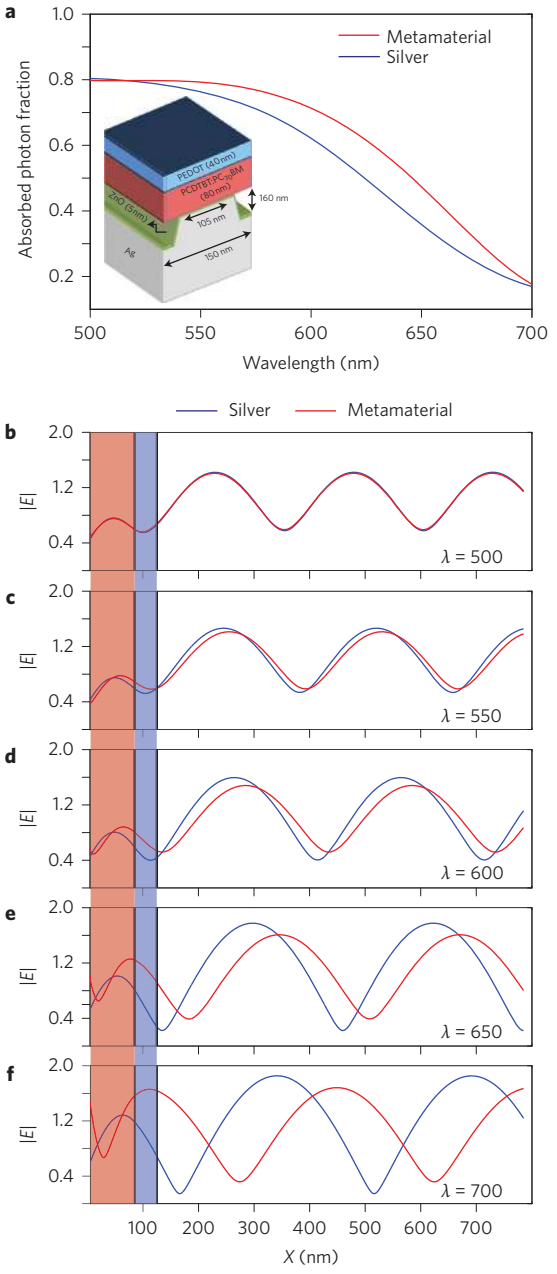

Figure 2 | Impact of metamaterial mirror on solar cell performance. **a**, Simulation of the optical properties of an organic solar cell with a metamaterial mirror, showing fraction of incident photons absorbed in an organic solar cell with a patterned silver magnetic mirror and a reference device with a flat mirror. Inset: one repeating unit cell of the device. **b**–**f**, Electric field profile across and above the devices with a metamaterial mirror (red) and a smooth silver mirror (blue). Simulations are shown for five wavelengths in the range 500–700 nm. The organic layers are colour-coded according to the same colour scheme as in **a**. Location $X = 0$ nm corresponds to the mirror surface.

field profiles are close to sinusoidal, as expected for a standing wave above a reflecting surface. This indicates that the dominant contribution to the absorption enhancement is not from the near-field effects that are used in some plasmon-enhanced photovoltaic devices. At the longer wavelengths (650–700 nm), the benefit of operating closer to resonance in the metamaterial-mirror device is mitigated by an increasingly unfavourable field overlap with the active medium. It can be seen that the maximum of the standing

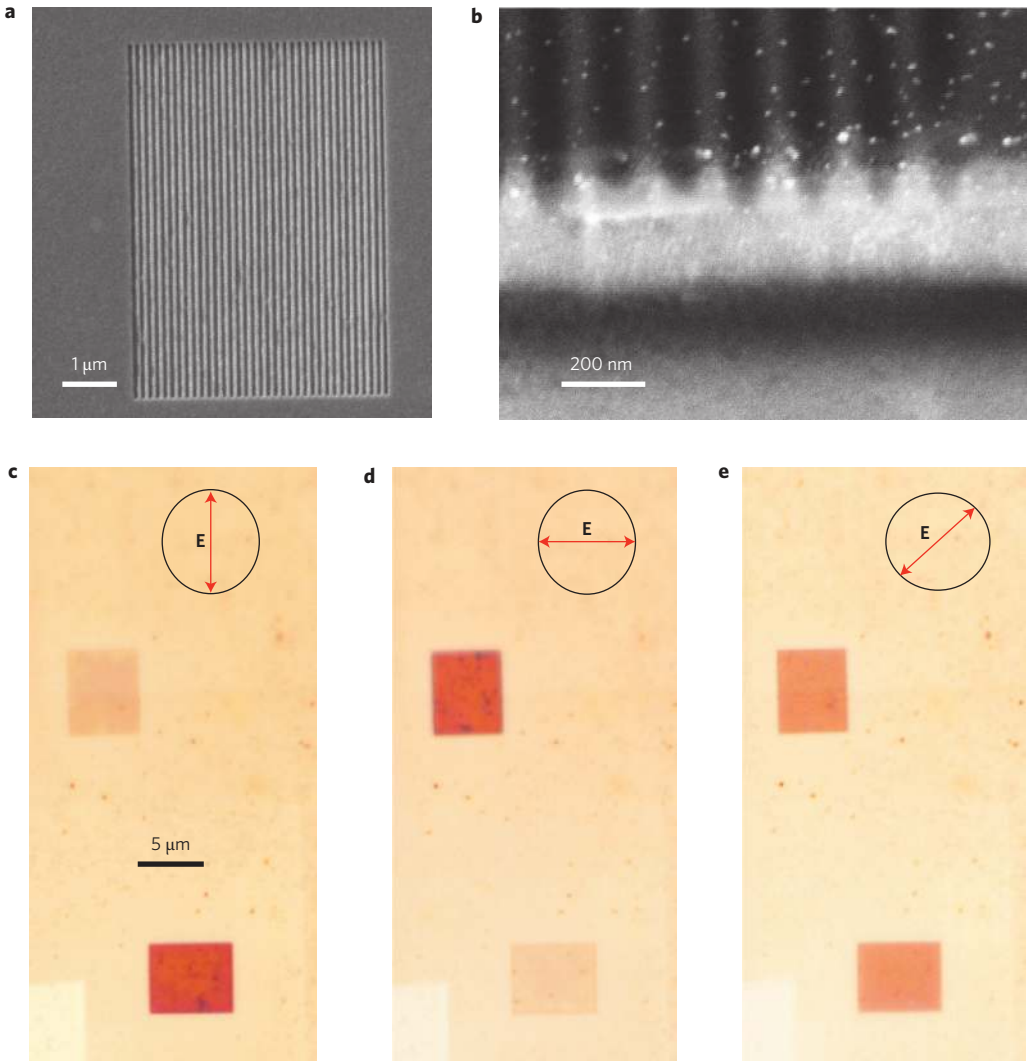

Figure 3 | Structural and optical characterization of fabricated devices. a, Top-view SEM image of a nanogroove array patterned into a smooth silver film. **b**, Cross-sectional SEM image of a fabricated device. **c–e**, Optical, white-light reflection images of a silver film covered with active polymer featuring two regions with subwavelength groove arrays in vertical (top) and horizontal (bottom) directions. The polarization direction of the illuminating light is shown as insets.

wave profile is slowly pushed out of the active layer as the wavelength increases. From this data set it is clear that the optimum absorption enhancements are attained when the reflection phase of the mirror provides a good compromise between maximizing the optical field overlap with the active layer and optimizing the resonant field enhancement derived from an optical resonance.

Structural and optical characterization

Figure 3a presents a scanning electron microscopy (SEM) image of the fabricated metamaterial mirror, which consists of a periodic array of grooves carved into a silver film by focused ion beam (FIB) milling. The cross-sectional SEM image in Fig. 3b shows that the grooves do not have perfectly straight side walls and sharp corners, and this was taken into account in the simulations and mirror design presented in Fig. 2a. The ZnO layer was grown on top of this mirror by means of atomic layer deposition (ALD). The PCDTBT:$PC_{70}BM$ and PEDOT layers were subsequently spin-coated onto the ZnO layer and can also be seen (faintly) in Fig. 3b (see Supplementary Methods for fabrication details).

Optical images of the silver back reflector are shown in Fig. 3c–e, and two rectangular areas with subwavelength groove arrays are clearly visible. The top rectangle has vertically aligned grooves and the bottom rectangle has horizontally arranged grooves. Under white-light illumination, the patterned areas appear substantially darker when the light is illuminated with TM polarization with the electric field orthogonal to the grooves. It can be seen that a rotation of the polarization direction results in a reversal of which pattern shows up darkest. For 45° polarization, both patterns show up equally dark. The darker appearance of the patterns for TM polarization is due to enhanced absorption in the active layer and some parasitic loss associated with the presence of the groove arrays. Some parasitic absorption in the metamaterial mirror cannot be avoided as its operation relies on the excitation of gap SPPs in the grooves of a lossy metal. Dark-field optical images taken from the same region indicate that the mirrors are of a high quality and do not produce significant diffuse scattering (Supplementary Fig. 5). This could also have led to a darker appearance. For the device, the key question is thus whether the benefits of having a metamaterial mirror with a desired optical field profile outweigh the detrimental optical losses. This can be analysed by photocurrent measurements.

Figure 4 illustrates how photocurrent maps of devices can be used to demonstrate the benefits of the metamaterial mirror. Figure 4a presents an SEM image of a silver film in a region that

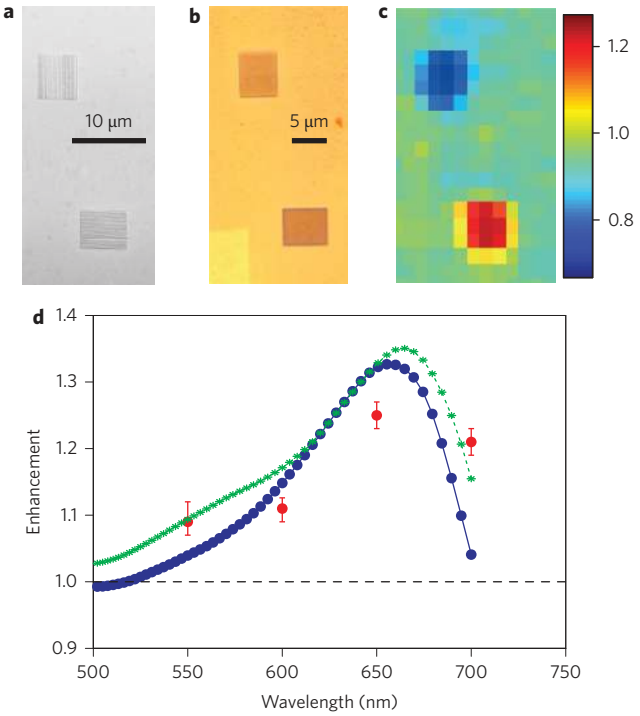

Figure 4 | Quantification of device performance enhancement due to presence of a metamaterial mirror. a,**b**, SEM (**a**) and optical (**b**) images of fabricated groove arrays with grooves in vertical (top) and horizontal (bottom) directions. **c**, Photocurrent enhancement map taken by raster-scanning a gently focused, 700-nm-wavelength illumination spot over the device. The ratio of the photocurrent obtained for vertical and horizontal polarizations of the incident light is plotted at each point. **d**, Spectral dependence of the photocurrent enhancement factor obtained for the magnetic mirror over the electric mirror. The red data points are the experimentally measured photocurrent enhancement factors and the error bars show the maximum and minimum values of the photocurrent measured within the patterned area. The blue line shows the enhancement factor obtained from the simulations in Fig. 2a. The green line provides the simulated enhancement factor for a metamaterial mirror in which every other groove in the original groove array is replaced with a slightly (10 nm) narrower groove. The dashed black line corresponds to an enhancement factor of 1 (that is, no enhancement) and is shown for reference.

features two areas with subwavelength groove arrays, one with vertical grooves (top) and one with horizontal grooves (bottom). Figure 4b shows an overview optical image in which the patterned areas are clearly visible, and Fig. 4c shows a photocurrent map from these same areas after devices were created on top of the metal. This map was created by raster-scanning a gently focused, 700-nm-wavelength laser spot over the device structures, taking the photocurrent for vertical and horizontal polarizations, and plotting the ratio of these photocurrents at each point. The resulting image provides a direct visualization of the polarization-dependent device performance in different regions. As expected, the unpatterned regions exhibit a polarization-independent response with a signal close to 1. The blue (red) region in the map indicates that a lower (higher) photocurrent is generated with vertical polarization versus horizontal polarization illumination of the grooved device areas. This visually shows the enhanced device performance due to the modified reflection phase in single device regions without concern for device-to-device variations. For photocurrent maps at other wavelengths see Supplementary Fig. 4. By averaging the photocurrent enhancement over the patterned device regions we find an enhancement of up to a factor of 1.2 for TM over TE illumination. Similar measurements were performed at other illumination wavelengths and are plotted in Fig. 4d. As predicted by the simulations in Fig. 2a, we find a broadband enhancement in the photocurrent that peaks near 650 nm based on the metamaterial mirror effect. These features agree with the predicted spectral enhancement (blue line) derived from the simulations shown in Fig. 2a. Differences between the experimental and simulated results are most likely caused by variations in the dimensions of the fabricated grooves. To explore this, we also simulated the spectral enhancement for a grating in which every other groove in the original groove array was replaced with a slightly (10 nm) narrower groove (green curve). The primary impact of this action was a broadening of the enhancement spectrum, which is also seen in the experiment.

Conclusions

We have shown the first beneficial use of a metamaterial mirror in an optoelectronic device operating in the visible spectral range. These mirrors offer a new approach to enhancing light absorption in optoelectronic devices that is distinct from a conventional light-trapping strategy aimed at redirecting incident light by means of Bragg scattering from a wavelength-scale grating. As the proposed mirror is metallic, it can provide good electrical access to active device layers. For this reason it could potentially eliminate the need for the electrically conductive and optically transparent spacer layers used in many thin planar devices (for example, indium tin oxide in thin-film solar cells or light-emitting diodes) today to optimize the electric field intensity inside a thin active semiconductor layer[32–36]. There is an active, ongoing search for better alternatives for such materials, as at present no material meets the many requirements in terms of low cost, earth abundance, high optical transparency and electrical conductivity, and favourable band alignment with other device layers[33]. Supplementary Fig. 3 illustrates some of the potential advantages of the metamaterial mirror over the use of transparent oxide spacers in terms of the improved electrical and optical properties. With the recent experimental demonstration of polarization-independent metamaterial mirrors in the visible[4,37], the presented concepts can be extended to devices for which an enhanced response to randomly polarized light is required. Mirrors have looked essentially the same for the last 8,000 years, but this work helps to show that it is worth reflecting on the potential opportunities that the discussed metamaterial mirrors may bring.

Methods

Device fabrication. Metamaterial-mirror devices were fabricated in a multistep process as follows. Silicon wafers with 300-nm-thick thermally grown oxide were used as a planar and smooth substrate. They were cleaned in several steps. First, they were brushed and sonicated with an Extran solution for 5 min, then rinsed with distilled water three times and sonicated in acetone for 5 min. In the final step, they were dried under flowing nitrogen gas. An ultrasmooth, optically thick silver film was then deposited onto the substrate using a germanium nucleation layer[38]. The nanogrooves were carved into these silver films by FIB milling with an FEI Strata 235DB dual-beam FIB/SEM tool. A 5-nm-thick ZnO layer was deposited on top of the grooved mirror by ALD at 150 °C using a Cambridge Nanotech Savannah using diethyl zinc (DEZ) and deionized water as precursors. The PCDTBT:$PC_{70}BM$ and PEDOT layers were deposited by spin coating. The spin coating speed for the PCDTBT was 2,500 r.p.m. and for PEDOT was 4,000 r.p.m. The solution concentration of PCDTBT (total solids) was 27.5 mg ml^{-1} and the solvent was dichlorobenzene. The PCDTBT:$PC_{70}BM$ ratio was 1:4. The thickness of each layer was measured on the flat area of the back reflector with a profilometer. After making the cell on top of the mirror, the top contact finger grid was deposited by thermal deposition of silver on the cell using a shadow mask. The fabrication of devices with inorganic semiconductors may leverage epitaxial light-off techniques[39] for thin semiconductor layers and subsequent layer transfer onto the metamaterial mirror. Alternatively, the metamaterial mirrors can be planarized to allow for subsequent device processing by first filling the grooved metal with a transparent medium and then polishing it by chemical mechanical polishing (CMP).

Photocurrent measurements. A white-light supercontinuum laser (Fianium) was used as the light source for the measurement. An acousto-optic tunable filter was

utilized to control the illumination wavelength. The polarization state of the laser beam was controlled by a set of polarization components including one polarizer and a half waveplate. The beam was focused onto the sample by a ×50 objective to a spot size of ~2 μm. The sample was mounted on a three-axis piezo stage (Physik Instrumente), which was used for accurate focusing and controlling the location of the beam spot on the sample. The motion of the piezo stage allowed for the creation of the photocurrent maps shown in the main text. To increase the signal-to-noise ratio the incident beam was chopped, and a source meter (Keithley) connected to a lock-in amplifier (Stanford Research Systems) measured the photocurrent. The photocurrent maps of the device were measured at wavelengths of 550, 600, 650 and 700 nm for two different polarizations. The ratio between the photocurrent maps of two polarizations was calculated by dividing the photocurrent maps by one another. The measured enhancement was not as high as predicted by simulation, which we believe to be due to additional optical losses (beyond those simulated for a smooth metal surface and tabulated optical properties) and possibly a reduced ability to extract charge from the patterned contact area. Dark-field images of the groove arrays were taken with a Nikon microscope before fabrication of the solar cell on top of the mirror. These images indicate that there is no significant scattering from the grooves, which means that the photocurrent enhancement is not caused by significant scattering/light trapping (Supplementary Fig. 5).

Received 29 November 2013; accepted 14 April 2014; published online 22 June 2014

References

1. Enoch, J. M. History of mirrors dating back 8000 years. *Optom. Vis. Sci.* **83,** 775–781 (2006).
2. Schwanecke, A. S. *et al.* Optical magnetic mirrors. *J. Opt. A Pure Appl. Opt.* **9,** L1–L2 (2007).
3. Genevet, P., Kats, M. A., Blanchard, R. & Capasso, F. Nanometre optical coatings based on strong interference effects in highly absorbing media. *Nature Mater.* **12,** 20–24 (2012).
4. Dotan, H. *et al.* Resonant light trapping in ultrathin films for water splitting. *Nature Mater.* **12,** 158–164 (2013).
5. Sievenpiper, D., Zhang, L. Z. L., Broas, R. F. J., Alexopolous, N. G. & Yablonovitch, E. High-impedance electromagnetic surfaces with a forbidden frequency band. *IEEE Trans. Microw. Theory Tech.* **47,** 2059–2074 (1999).
6. Kuester, E. F., Mohamed, M. A., Piket-May, M. & Holloway, C. L. Averaged transition conditions for electromagnetic fields at a metafilm. *IEEE Trans. Antennas Propag.* **51,** 2641–2651 (2003).
7. Biener, G., Niv, A., Kleiner, V. & Hasman, E. Metallic subwavelength structures for a broadband infrared absorption control. *Opt. Lett.* **32,** 994–996 (2007).
8. Luukkonen, O. *et al.* Simple and accurate analytical model of planar grids and high-impedance surfaces comprising metal strips or patches. *IEEE Trans. Antennas Propag.* **56,** 1624–1632 (2008).
9. Zhao, Y., Alù, A. & Engheta, N. Homogenization of plasmonic metasurfaces modeled as transmission-line loads. *Metamaterials* **5,** 90–96 (2011).
10. Moreau, A. *et al.* Controlled-reflectance surfaces with film-coupled colloidal nanoantennas. *Nature* **492,** 86–89 (2012).
11. Pors, A. & Bozhevolnyi, S. I. Efficient and broadband quarter-wave plates by gap-plasmon resonators. *Opt. Express* **21,** 2942–2952 (2013).
12. Kildishev, A. V., Boltasseva, A. & Shalaev, V. M. Planar photonics with metasurfaces. *Science* **339,** 1232009 (2013).
13. McVay, J., Engheta, N. & Hoorfar, A. High impedance metamaterial surfaces using Hilbert-curve inclusions. *IEEE Microw. Wirel. Components Lett.* **14,** 130–132 (2004).
14. Yang, F. Y. F. & Rahmat-Samii, Y. Reflection phase characterizations of the EBG ground plane for low profile wire antenna applications. *IEEE Trans. Antennas Propag.* **51,** 2691–2703 (2003).
15. Prosvirnin, S. L. & Zheludev, N. I. Polarization effects in the diffraction of light by a planar chiral structure. *Phys. Rev. E* **71,** 037603 (2005).
16. Papakostas, A. *et al.* Optical manifestations of planar chirality. *Phys. Rev. Lett.* **90,** 107404 (2003).
17. Fedotov, V. A., Mladyonov, P. L., Prosvirnin, S. L. & Zheludev, N. I. Planar electromagnetic metamaterial with a fish scale structure. *Phys. Rev. E* **72,** 056613 (2005).
18. Fedotov, V. A., Rogacheva, A. V., Zheludev, N. I., Mladyonov, P. L. & Prosvirnin, S. L. Mirror that does not change the phase of reflected waves. *Appl. Phys. Lett.* **88,** 091119 (2006).
19. Nanfang, Y. *et al.* Light propagation with phase discontinuities: generalized laws of reflection and refraction. *Science* **334,** 333–337 (2011).
20. Kildishev, A. V., Shalaev, V. M., Boltasseva, A., Emani, N. K. & Ni, X. Broadband light bending with plasmonic nanoantennas. *Science* **335,** 427 (2012).
21. Pors, A. *et al.* Optical transparency by detuned electrical dipoles. *New J. Phys.* **13,** 023034 (2011).
22. Schuck, P. J., Zolotorev, M., Polyakov, A. & Padmore, H. A. Collective behavior of impedance matched plasmonic nanocavities. *Opt. Express* **20,** 7685 (2012).
23. Miyazaki, H. T. & Kurokawa, Y. How can a resonant nanogap enhance optical fields by many orders of magnitude? *IEEE J. Sel. Top. Quantum Electron.* **14,** 1565–1576 (2008).
24. Pardo, F., Bouchon, P., Haïdar, R. & Pelouard, J-L. Light funneling mechanism explained by magnetoelectric interference. *Phys. Rev. Lett.* **107,** 093902 (2011).
25. Eriksen, R. L. *et al.* Plasmonic black gold by adiabatic nanofocusing and absorption of light in ultra-sharp convex grooves. *Nature Commun.* **3,** 969 (2012).
26. Shin, H., Yanik, M. F., Fan, S., Zia, R. & Brongersma, M. L. Omnidirectional resonance in a metal–dielectric–metal geometry. *Appl. Phys. Lett.* **84,** 4421 (2004).
27. Liu, J. S. Q. & Brongersma, M. L. Omnidirectional light emission via surface plasmon polaritons. *Appl. Phys. Lett.* **90,** 91116 (2007).
28. Mann, S. a. & Garnett, E. C. Extreme light absorption in thin semiconducting films wrapped around metal nanowires. *Nano Lett.* **13,** 3173–3178 (2013).
29. Hägglund, C. & Apell, P. Plasmonic near-field absorbers for ultrathin solar cells. *J. Phys. Chem. Lett.* **3,** 1275–1285 (2012).
30. Thongrattanasiri, S., Koppens, F. H. L. & García de Abajo, F. J. Complete optical absorption in periodically patterned graphene. *Phys. Rev. Lett.* **108,** 047401 (2012).
31. Beiley, Z. M. *et al.* Morphology-dependent trap formation in high performance polymer bulk heterojunction solar cells. *Adv. Energy Mater.* **1,** 954–962 (2011).
32. Heeger, A. J. *et al.* Bulk heterojunction solar cells with internal quantum efficiency approaching 100%. *Nature Photon.* **3,** 297–302 (2009).
33. Kim, J. Y. *et al.* New architecture for high-efficiency polymer photovoltaic cells using solution-based titanium oxide as an optical spacer. *Adv. Mater.* **18,** 572–576 (2006).
34. Kim, J. Y. *et al.* Efficient tandem polymer solar cells fabricated by all-solution processing. *Science* **317,** 222–225 (2007).
35. Roy, A. *et al.* Titanium suboxide as an optical spacer in polymer solar cells. *Appl. Phys. Lett.* **95,** 13302 (2009).
36. Gilot, J., Barbu, I., Wienk, M. M. & Janssen, R. A. J. The use of ZnO as optical spacer in polymer solar cells: theoretical and experimental study. *Appl. Phys. Lett.* **91,** 113520 (2007).
37. Rostami, H., Abdi, Y. & Arzi, E. Fabrication of optical magnetic mirrors using bent and mushroom-like carbon nanotubes. *Carbon* **48,** 3659–3666 (2010).
38. Logeeswaran, V. J. *et al.* Ultrasmooth silver thin films deposited with a germanium nucleation layer. *Nano Lett.* **9,** 178–182 (2009).
39. Gordon, I. *et al.* Three novel ways of making thin-film crystalline-silicon layers on glass for solar cell applications. *Sol. Energy Mater. Sol. Cells* **95,** S2–S7 (2011).

Acknowledgements

This publication was based on work supported by the Center for Advanced Molecular Photovoltaics (CAMP) funded by King Abdullah University of Science and Technology (KAUST) under award no. KUS-C1-015-21. It was also supported by the Department of Energy (grant no. DE-FG07ER46426). The authors thank P. Landreman and V. Esfandyarpour for discussions.

Author contributions

M.E. and M.L.B. conceived the idea of using metamaterial mirrors in optical devices. M.E. performed the optical simulations. M.E. and E.C.G. fabricated and tested the devices. All authors were involved in analysing the data and writing the manuscript.

Additional information

Supplementary information is available in the online version of the paper. Reprints and permissions information is available online at www.nature.com/reprints. Correspondence and requests for materials should be addressed to M.L.B.

Competing financial interests

The authors declare no competing financial interests.